DOI: 10.13009/EUCASS2019-504

Computational Design of a CubeSat Compatible Re-entry Capsule

Mohammad Yousefi and Cliff Wachiuri** and Vishva Plaitharathna*** and Mahmoud Hamdy**** and Boutheina Tlili***** and Mihail Barbosu****** and Wael Abdel Samad *******

**Rochester Institute of Technology – Dubai - UAE*

mmy3147@rit.edu

***Rochester Institute of Technology – Dubai - UAE*

cew9765@rit.edu

**** Rochester Institute of Technology – Dubai - UAE*

vbp2615@rit.edu

***** Rochester Institute of Technology – Dubai - UAE*

mhh4813@rit.edu

****** Rochester Institute of Technology – Dubai – UAE*

bktcad@rit.edu

******* Rochester Institute of Technology – New York – USA*

mxbsma@rit.edu

******** Rochester Institute of Technology – Dubai - UAE*

wascad@rit.edu

Abstract

CubeSats have revolutionized space experimentation by providing a small low-cost platform which has as a result enabled many who did not have access to space to now be able to easily perform experiments. However, one of the main shortcomings of CubeSats is the limited availability for on board sensing equipment and limited power available to perform certain types of experiments for long periods of time in orbit. This paper aims to design a modular re-entry capsule compatible with 2U+ CubeSats and using CFD and structural simulation methods to allow a safe re-entry from Low earth orbits.

1. Introduction and objectives

The concept of CubeSats began in the year 1999, as a collaboration between two professors at the California Polytechnic State University and Stanford University's Space Development laboratory as a way of providing university students with affordable access to outer space experiments [1]. CubeSats are small cubic and cuboid satellites which are built within strict standards set by NASA [2]. This allows them to be launched alongside larger space payloads at a fraction of the cost of sending them to space on their own. This lower cost has allowed many companies and educational and research institutions to launch CubeSats to perform various space experiments [2].

However, this low-cost system has its drawbacks. Firstly, they are currently designed in a way that they will burn up in the atmosphere at the end of their mission upon re-entry. This is done to eliminate the risk of accidental damage to life or property since the re-entry will not be controlled. This design method means that all the experiments must take place

DOI: 10.13009/EUCASS2019-504

during the mission time of the satellite and all data shall be collected and transmitted to a ground station during the mission time of the satellite. Failure to do so will cause the entire experiment to fail [2]. Due to their size limitations, CubeSats are limited in the experiments they can perform and the quality and quantity of data they can provide. They are often limited with the sensors they can have onboard and the limited power they have in order to power them. One method that can be employed to augment the capability of CubeSats is the incorporation of a sample return capsule. This will allow for sample analysis after mission completion or incorporation of high capacity data storage devices on board which will allow the CubeSat to record high fidelity data that can be collected and analyzed at a later time. Thus eliminating the need to transmit the information during mission time, reducing the required operating power of the satellite.

Design of sample return capsules and re-entry craft has been a challenge which has been tackled ever since the beginning of the space era and the design of the CORONA satellite sample return buckets [3]. Ever since the development of such craft, one principle has been the key to the design of all sample return re-entry craft, and that is their blunt shape. This blunt design of re-entry craft has been instrumental in generating a stronger shockwave thus causing greater heat dissipation and lower heat transfer to the body of the craft [4]. Since then, sample return and crew return capsules have been using the same spherically capped blunt shape [5]. The greatest challenge for sample return craft however is overcoming the excessive heat which is generated during re-entry. For ballistic re-entry cases, ablative material are shown to be ideal. Newer polymeric ablative materials such as the Phenolic Impregnated Carbon Ablators (PICA) are often used for such cases due to their very high resistance and low densities [6]. Various programs such as the MIRKA 2 satellite and NASA's REBR program and the CAPE program have worked on creation of cube sat sized re-entry devices [7] [8] [9]. Further approaches such as inflatable aero shells have been explored [10]. However currently no design exists which allows for the completion of all types of experiments in space. This paper aims to provide a design and numerical simulation of a modular re-entry capsule alongside its integrated electronic system which allows for a climate controlled and pressurized compartment for all experiment types.

2. Craft Geometry

The craft has been designed to fit in a 2U CubeSat enclosure as shown in Figure 1. With tolerances considered to allow for additional equipment to fit in the enclosure to allow for fixation of the module to the frame and jettisoning equipment.

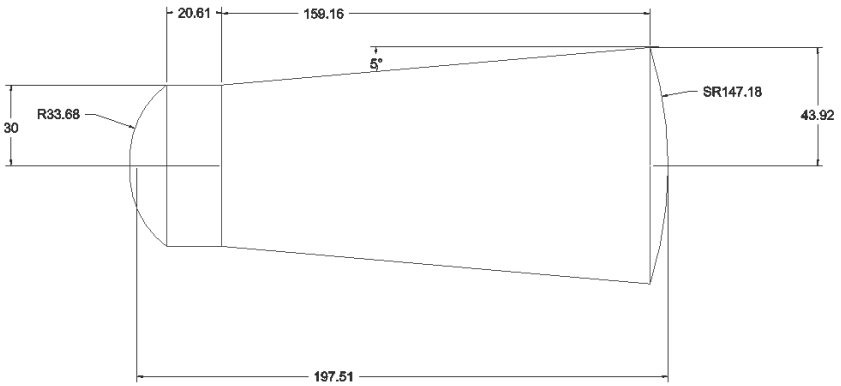

Figure 1 : Dimensions of the re-entry capsule (all dimensions in mm)

DOI: 10.13009/EUCASS2019-504

The nose radius and the backwards sweep angle were chosen in order to create the most detached shockwave and least aerothermal load on the nose and side of the craft while maximizing its internal volume. A conic shape on the rear was also added to reduce heating on the rear of the craft during re-entry.

3.Aerothermal Simulation

3.1 Trajectory model

The analysis of the trajectory begins at 80 km above the mean sea level, and the atmosphere is modelled using the 1976 US Standard atmosphere [11]. The analysis is performed with the expectation that the re-entry will occur with a constant -20° angle and at a velocity of 7500 m/s. These values were chosen based on analysis of various low earth orbit CubeSat missions and such conditions were seen to be among the most extreme which can be experienced by an uncontrolled CubeSat re-entering the atmosphere. The following equations characterize the dynamics of the craft:

$$-D + Wsin(\theta) = m\frac{dV}{dt} \quad (1)$$

where D is the acting drag force on the craft, W is the weight of the craft, θ is the re-entry angle and m is the mass of the craft.

This equation assumes a constant gravitational force throughout re-entry. The craft has an estimated drag coefficient of 1.53 in hypersonic speeds and assuming a full 2U load of 2.6 kg, this yields a constant ballistic parameter of 300 kg/m^2. The acquired trajectory information can be seen in Figure 2.

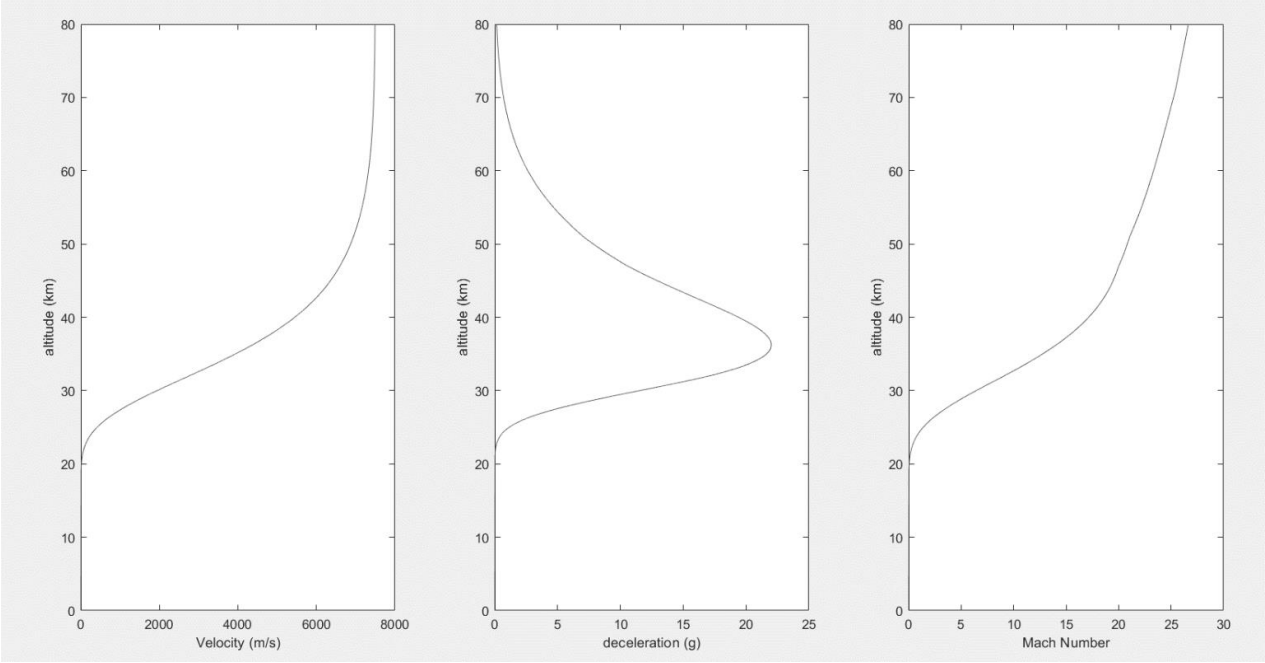

Figure 2 : Variation of velocity, deceleration and Mach number along the re-entry trajectory

3.2 Analysis of the stagnation point heating

Multiple models and methods exist to calculate the stagnation point heating on re-entry craft re-entering the atmosphere. Various engineering models exist which have proven themselves to be accurate when compared to experimental results. There are two main types of heat transfer to the craft during re-entry: the convective heat flux and the radiative heat flux.

DOI: 10.13009/EUCASS2019-504

However, and since the entry velocity is less than 9000 m/s, the radiative heat flux can be safely ignored [12]. Among the engineering models are those which have been formulated by Sutton and Graves, Tauber and Detra and Hidalgo. The Sutton and Graves and Tauber models are formulated as follows [5]:

$$\dot{q}_{\,convective} = K\left(\frac{\rho}{R_n}\right)^{\frac{1}{2}} V^3 \tag{2}$$

Where ρ is the atmospheric density, R_n is the nose radius and V is velocity of the craft. *K* is an atmospheric constant which for the case of Sutton and Greaves has a constant value of $1.742*10^{-4}$ and for Tauber it has a value of $1.83*10^{-4}$ [13] [5]. Furthermore, the Detra and Hidalgo Model is formulated as follows [14]:

$$q_s = 5.16 * 10^{-5}\left(\frac{\rho}{R_n}\right)^{\frac{1}{2}} V^{3.15} \tag{3}$$

While all three models correlate, the Detra and Hidalgo Formulation yields a higher value around the point of maximum heat transfer, thus this model will be used as a basis for further analysis.

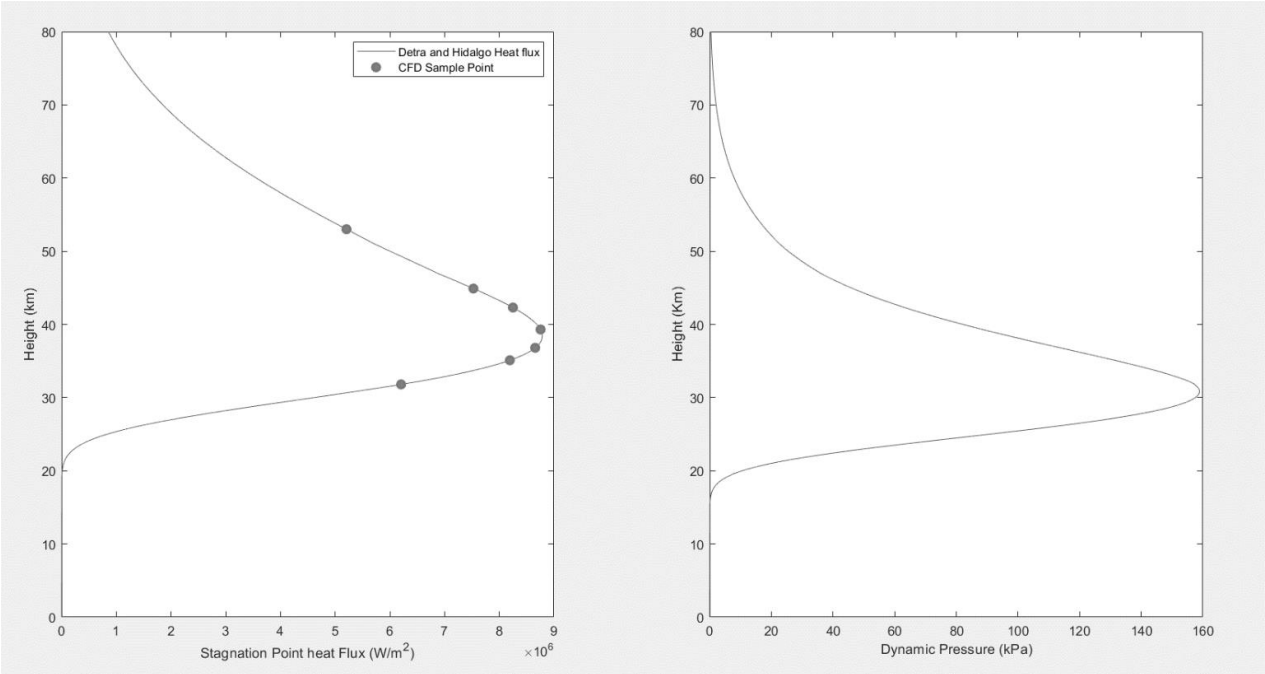

Figure 3 : Variation of Aerothermal Forces along the re-entry trajectory

In Order to acquire more detailed full field information regarding the craft at different times during re-entry the craft was simulated in ANSYS FLUENT. A commercially software which is known to be able to accurately calculate fluid flows in hypersonic conditions [15] [5]. The simulation was performed in steady state using 2D axisymmetric conditions to ease the computing requirements. The air mixture was modelled based on the built-in air mixture in FLUENT, using the AUSM formulation and the 5 equation Reynold's Stress model for turbulence modelling. A fine mesh comprising of 14775 cells was generated around the craft as shown in Figure 4, with the boundary conditions indicated in Figure 5.

DOI: 10.13009/EUCASS2019-504

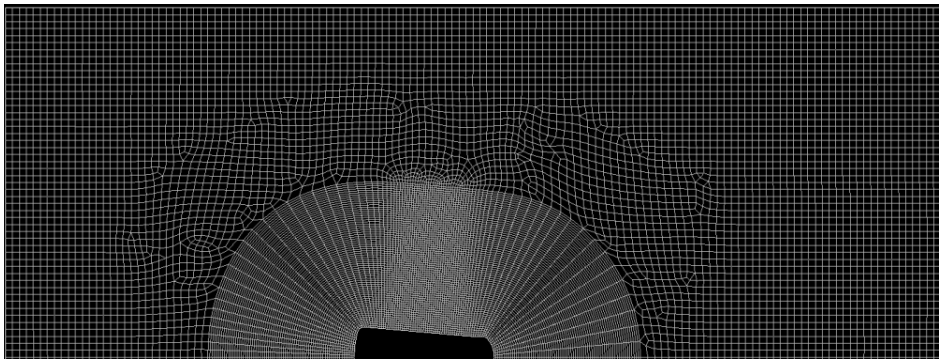

Figure 4 - Mesh Setup for CFD

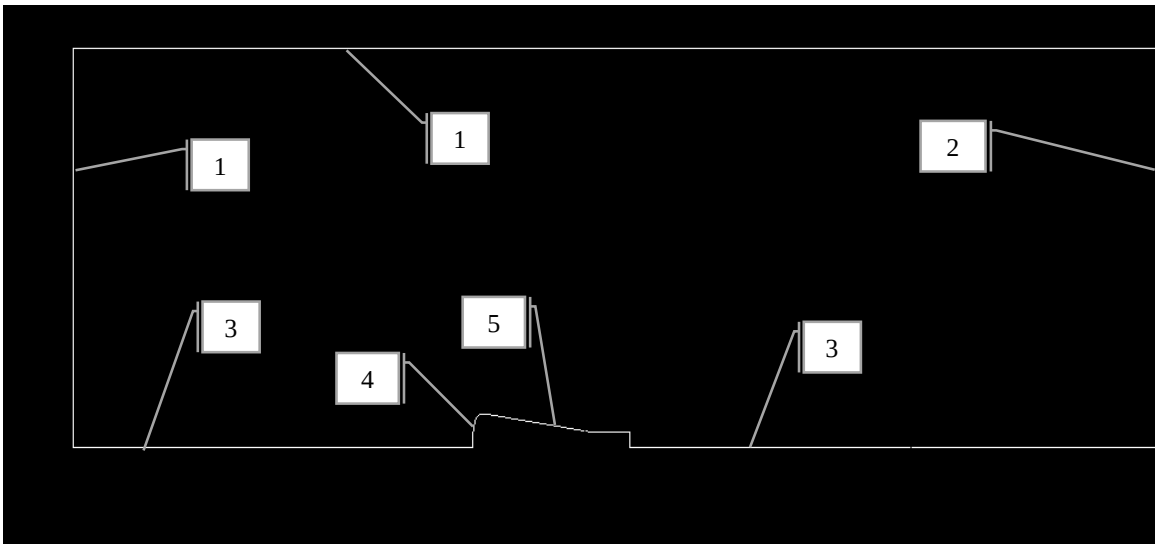

Figure 5 - CFD Boundary conditions. 1- Pressure Far Field 2-Pressure Outlet (not shown) 3-Axis 4&5 - Wall Condition

The wall was defined as a no slip wall with a constant temperature of 300K [14] [5]. The simulation was then carried out based on the conditions at the different CFD Sample Points as can be seen in Figure 3.

Table 1 - Comparison between CFD and Theoretical results

Altitude (Km)	53	44.9	42.3	39.3	36.8	35.1	31.8
Detra and Hidalgo heat Flux (W/m^2)	5.21E+06	7.53E+06	8.25E+06	8.75E+06	8.66E+06	8.19E+06	6.21E+06
CFD Heat Flux (W/m^2)	8.01E+06	1.41E+07	1.62E+07	1.71E+07	1.41E+07	1.13E+07	2.85E+06
Error (%)	54	87	96	95	63	38	54

As seen in Table 1 and Figure 6, the values acquired from the CFD calculation are higher than the predicted value by an average of 70% while at the final sample point the CFD value is lower by 54% . This can be due to both the geometry of

DOI: 10.13009/EUCASS2019-504

the craft and other effects such as the fully catalytic conditions on the wall [5]. Thus taking a more conservative approach to the design, further design steps will assume an average heat flux of 17MW/m^2 at the stagnation point of the craft. While detailed Ablation simulation could be done in order to fine tune the thickness of the TPS for each mission case, analysis done by Cardente et. Al. on a case with similar heating concluded that 4 cm. of TPS will be adequate for a safe re-entry [5].

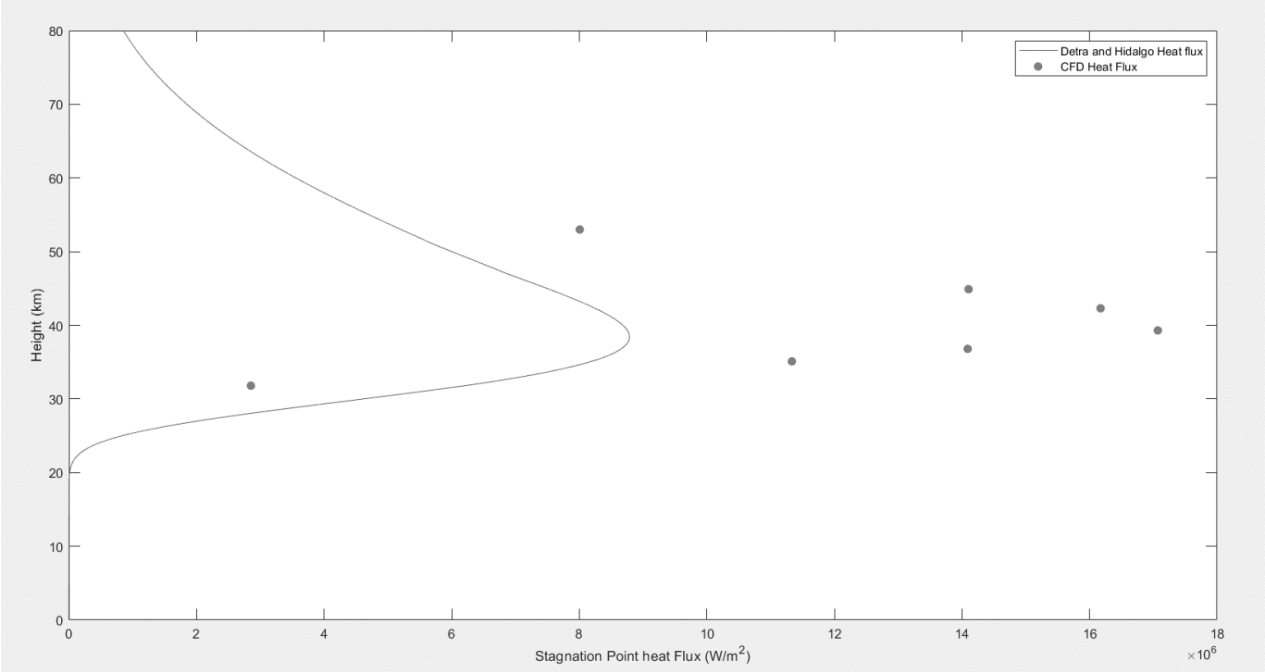

Figure 6 : Theoretical and CFD Heat Fluxes

4.Hull Design

4.1 Materials and internal Modelling

The craft is designed to consist of three layers of materials, bonded on top of each other. The outer most layer being PICA while supported by a Titanium Alloy (Ti 10 V2 Fe3 AL) with the addition of an aerogel derivative, commercially available WDS Ultra for additional insulation during re-entry [16] [17] [18]. The craft was furthermore designed to be able to have a pressurized chamber of a constant 1 Atm. pressure to allow for pressure sensitive experimentation, as shown in Figure 7

DOI: 10.13009/EUCASS2019-504

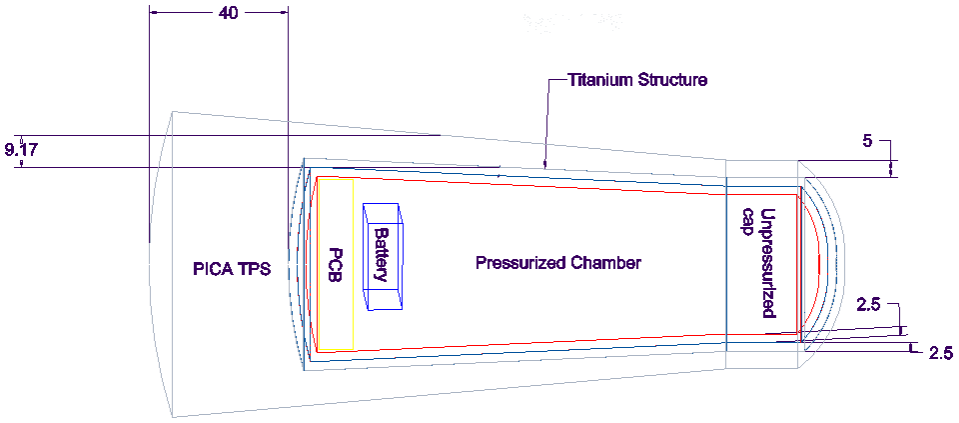

Figure 7 : Internal Structure of the capsule (dimensions in mm)

The antenna will be housed in the unpressurized section of the craft alongside fixtures and equipment for detachment of the cap during re-entry, this will allow the antenna to extend and be able to transmit location information after successful re-entry. The pressurization will be done through the incorporation of a cap and a labyrinth seal in cases where it is required.

4.2 Pressure Simulations

The simulations performed on the craft were only done on the Titanium and WDS Ultra layers, given that they are the layers that will ensure structural rigidity of the craft throughout its mission. Furthermore, PICA could not be fully simulated given a lack of material information. The simulations were done in 3D in ANSYS Workbench using the Mechanical APDL Solver. The two materials were set to be bonded with no friction between them. The first test which was performed was a steady state test with 1 atm of internal pressure and vacuum on the outside, Figure 8.

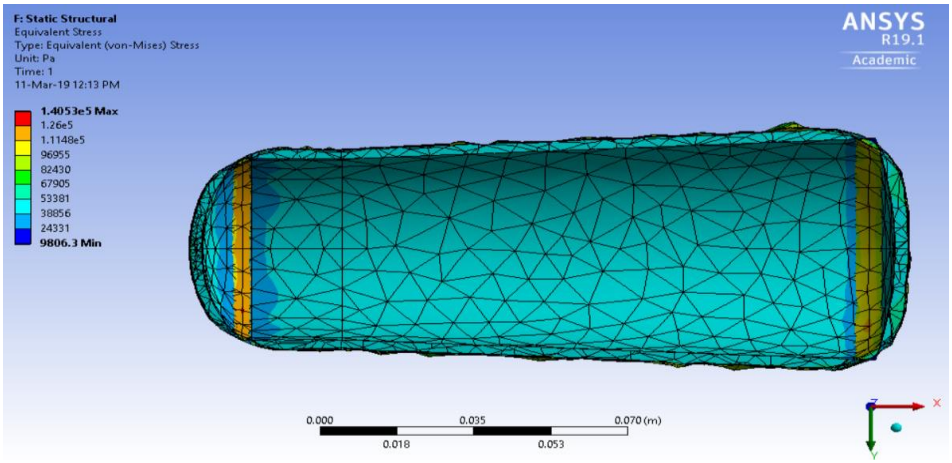

Figure 8 : Principal (Von Mises) stresses based on pressurization in Vacuum

The maximum equivalent stress (Von Mises) was $1.4053*10^5$ Pa and it was seen that the edges are subjected to larger deformation compared to the rest of the body, followed by the principal (Von Mises) stress of 84448 Pa, built up around the same area. The total deformation however is $2.4785*10^{-9}$ m. Both the strains and stresses in this case are well below the tolerances for all the materials [16] [17] [19]. Further transient simulations were performed to simulate the

DOI: 10.13009/EUCASS2019-504

aerodynamic forces acting on the craft during its full course of re-entry using information gathered from the CFD analyses, in this case, while the stresses were higher than that of the previous simulation, they were still well below the stress and strain limits of the materials, Figure 9.

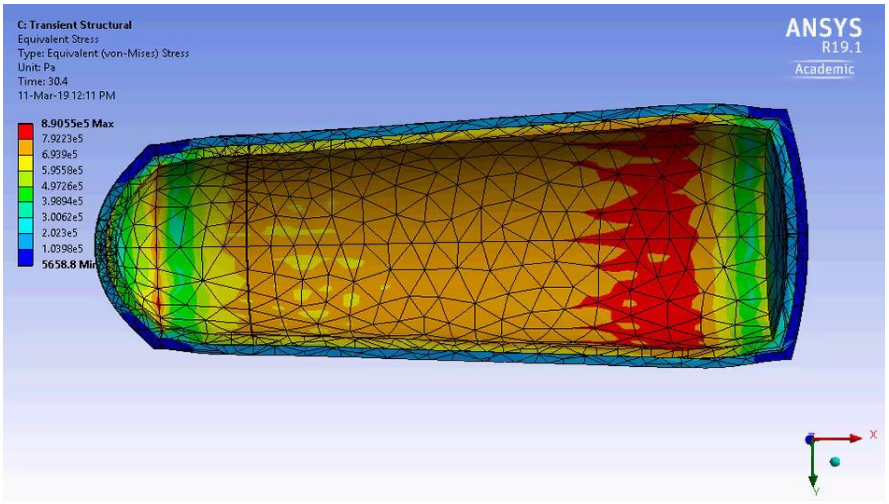

Figure 9 : Peak Equivalent (Von Mises) Stresses During Re-entry

4.2 Impact Simulations

The structural components of the craft were also subjected to impact testing using the ANSYS Explicit Dynamics module to test their integrity in case of impact on hard ground. The Craft was tested in 3D while impacting a fixed concrete surface at a speed of 20 m/s, which is around the nominal descent rates of high-speed model rockets of similar mass. Standard Earth gravity was included in the simulation along with an additional 3Kg of mass being added to simulate full load of the craft.

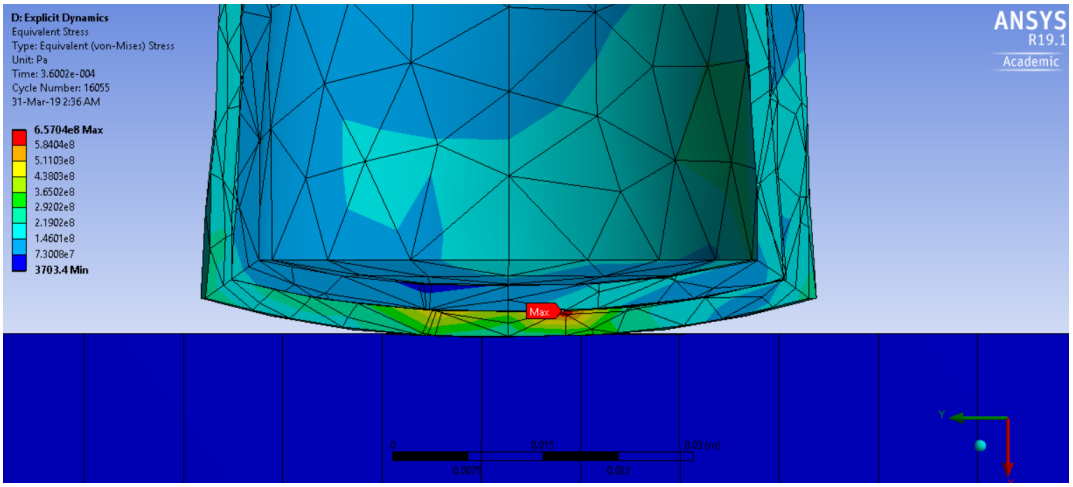

Figure 10 : Equivalent Von Mises stresses at point of impact (arrow denotes the point of maximum stress)

DOI: 10.13009/EUCASS2019-504

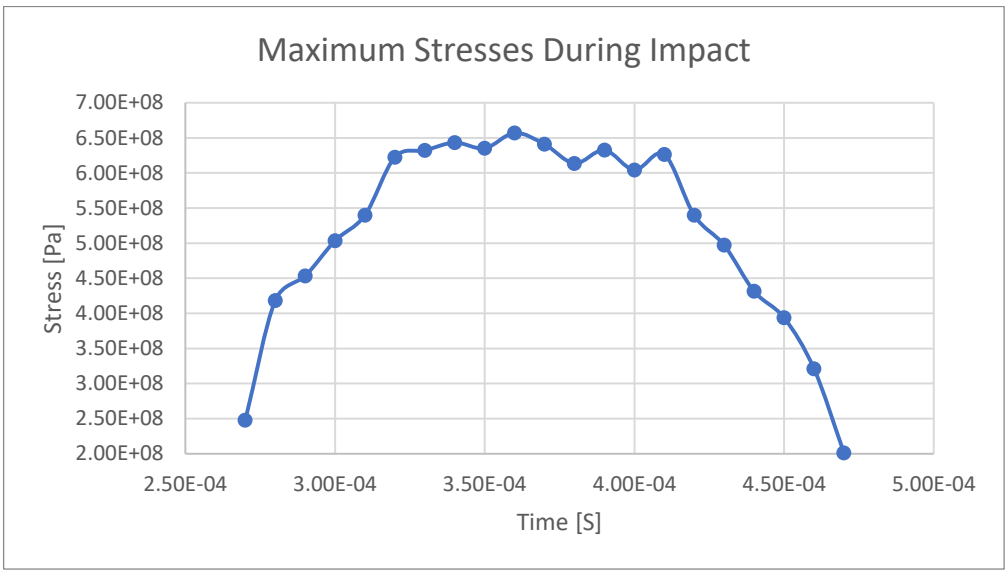

Figure 11 : Maximum Von Mises stresses during impact

The maximum stress occurred on the Titanium hull as shown in Figure 10 and on the bonding point between and had a value of $6.57*10^8$ Pa as shown in Figure 11, this value leaves the Titanium hull to have a factor of safety of 1.92 given that none of the PICA layer will be left to further absorb the impact, this it can be safely said that full integrity can be maintained in the craft even with a structural titanium layer of 2.5mm thickness.

4.3 Thermal Simulation

In order to simulate the internal temperature of the craft during re-entry, the bond line temperature data of a similar re-entry case and design were used to optimize the internal insulative layer thicknesses [5]. From the CFD results it was seen that the side and rear wall heat fluxes account for less than 10% of the heat flux and thus they will not experience much heating. However the stagnation wall temperature can reach temperatures up to 200° C during a shallow re-entry with similar peak heating as discussed in [5]. The calculated bond line temperatures were used throughout a 600 second flight time and it was determined that the initial 2.5mm insulation thickness on the stagnation wall will prove itself to be inadequate as the internal temperature of the craft can reach up to 195° C during re-entry. It was determined that the insulation thickness should be optimized to reach a maximum temperature of 70° C to ensure the safety of onboard electronics and possible bio experiments during re-entry. The thickness of the insulation was optimized using the ANSYS MOGA Algorithm with an objective temperature of 70° C and upper limit temperature of 80° C based on the temperature response chart generated after simulation of various insulation thicknesses shown in Figure 12.

DOI: 10.13009/EUCASS2019-504

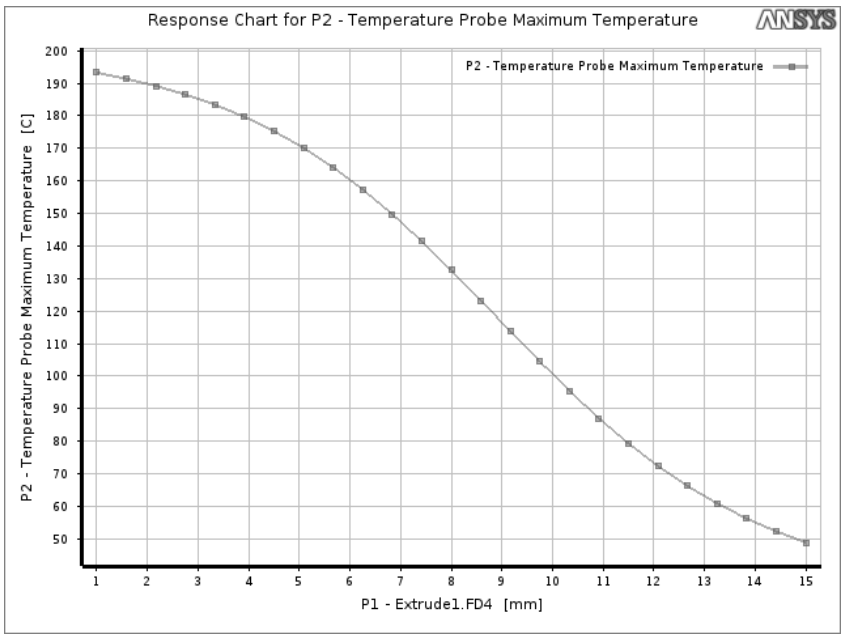

Figure 12 : Temperature response based on insulation thickness

The thickness of the lower wall WDS Ultra insulation on the stagnation facing wall was then determined to be best between 12.1 and 12.3 mm yielding maximum temperatures between 72° C to 70° C respectively.

5.Electronics Design

5.1 Hardware Architecture

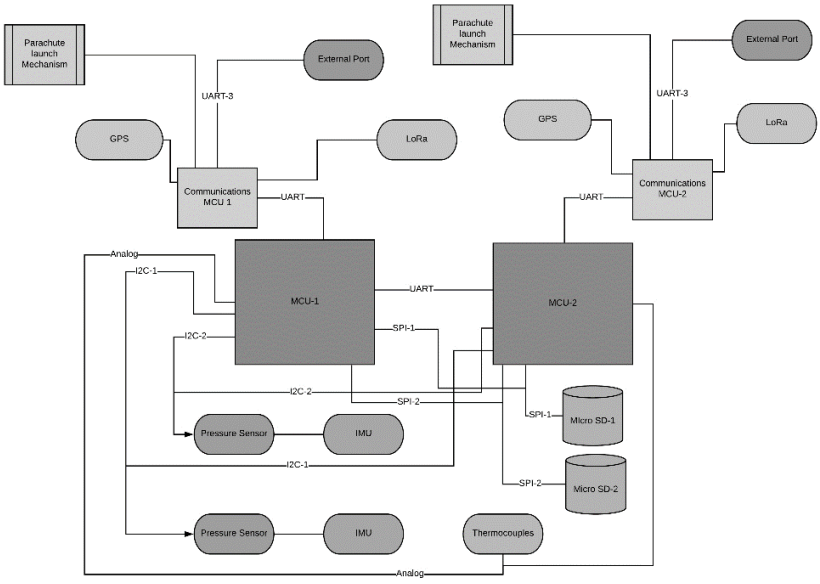

Figure 13 : Electronics architecture of the module

DOI: 10.13009/EUCASS2019-504

The electronics architecture of the Asteria Module as shown in Figure 13, incorporates the use of various microcontrollers, sensors, and memory devices. The main architecture incorporates the use of absolute redundancy whereby, there are two duplicate electronic systems, controlled by two microcontrollers, each capable of interfacing with all the sensors, memory devices and communication systems.

5.2 Power Consumption

The module is designed to consume a maximum of 60uW in standby mode. This promotes the use of a smaller battery for the longest periods of time. The device will be in deep-sleep mode for most of the time before re-entry, unless upon a communication request from the electronics systems in the CubeSat's main module. The peak power consumption is targeted at 0.7W during communication with GPS satellites and Long-Range Wide Area Networks (LORAWAN), and they are to be turned off when the module is not in re-entry mode.

5.3 Communication with the host satellite

The module can communicate with the host CubeSat. This will be through a 3- wire UART interface link of 921600kbps. This will allow for the host to interface with the device's sensors, or to store information, such as images captured from space which would be retrieved on re-entry into earth.

5.4 PCB Design

This design incorporated a 50 x 55mm dual layer PCB built on an FR4 substrate with a thickness of 1.6 mm Shown in Figure 14. The design was built using EasyEDA PCB design tool by first creating multiple schematics with all the components. From the schematic, the components were then placed strategically onto a PCB layout. This was to ensure that RF antennas had the shortest route to the transceiver without any interference nearby from SPI data lines running at 40MHz. After placement, a local routing server was run so as to create and optimize the routing of tracks connecting the various components onto the PCB. However, several constraints were put onto the design, such as a track width of 0.16mm, a clearance of 0.2mm.

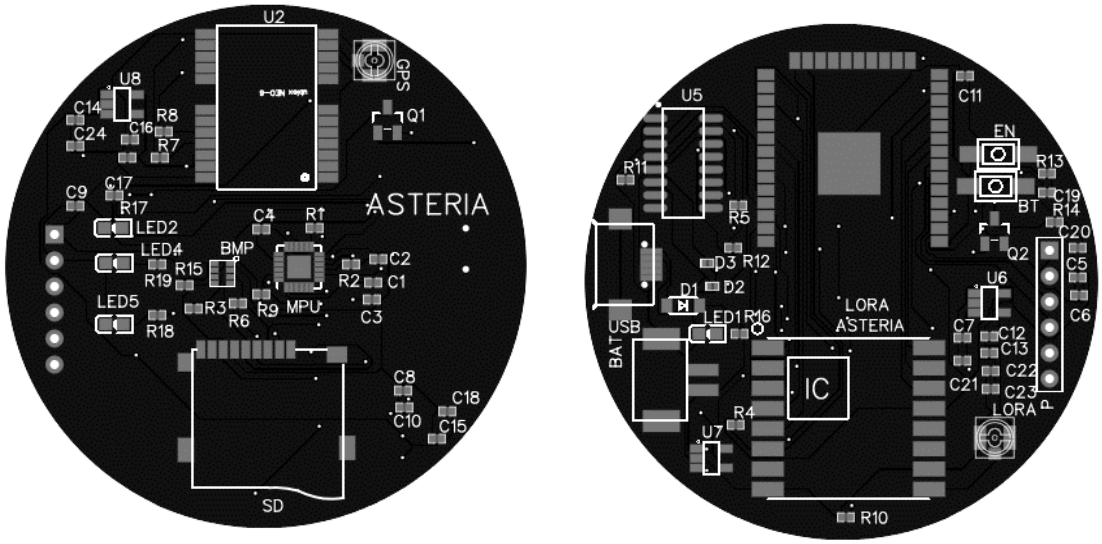

Figure 14 : PCB Design (Front and Rear)

DOI: 10.13009/EUCASS2019-504

5.5 Components List

1. Inertial Measurement Units for acceleration and attitude measurement
2. Barometric sensors to detect altitude and cabin pressurization.
3. Thermocouples to measure temperature on the surface of the module
4. Pressure sensors to measure static pressure.
5. ESP-WROOM32 MCU capable of deep sleep mode.
6. U-Blox GPS MCU.
7. STM32 LoRa Transceiver MCU.
8. 16GB SD Cards.

5.6 Satellite and Ground Based Communications

The device is planned to use Global Positioning Satellite system for position identification.

Iridium satellite communication has also been considered but, due to high costs and power consumption, it may be difficult to implement. However, it is most efficient in transmitting the location in case the module lands in a very remote area.

Long Range Wide Area Networks (LORAWAN) is the communication system of choice due to its robustness, long range of about 20km, and readily available off the shelf modules [20]. The communication hardware was tested as shown in Figure 15 to show a 2.5Km Non-line of sight ability to transmit packets while operating at 50% transmit power.

Figure 15 : Test Radius of LoRa (The radius line denotes the direction of the performed test)

DOI: 10.13009/EUCASS2019-504

5.7 Software Architecture

5.7.1 Conceptual Model of communication Between the Asteria Module and the Host Device

The module is designed to interface with the host device vis UART, a medium-speed, asynchronous serial communication. It will be a three-tier topology shown in Figure 16, the lowest being the physical layer that transmits data over two wires, a data link layer for enforcing the communication protocol to be used, and an application layer, which will allow for hardware-abstracted functions to be called from the host device to the module, such as access to sensor data and data storage to the SD cards.

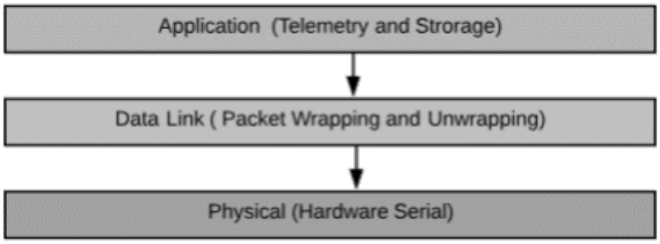

Figure 16 : Communication infrastructure conceptual model

5.7.2 Redundancy

The primary microcontroller communicates regularly with the backup microcontroller, by performing a complex AES function and returning a value that will be cross-checked by the backup microcontroller with a predefined value which would be the correct result. In case of failure, the backup microcontroller would then take over the processes. In addition, the backup microcontroller will start operating in case the primary microcontroller is unable to perform primary functions such as the loss of an interface to sensors. In case of partial failure of both, the microcontrollers will have the ability to complement each other's functions as the last redeeming factor.

5.7.3 Multithreaded Architecture

The architecture of the microcontrollers will involve the use of a multi-threaded Real-Time Operating System(FREERTOS) shown in Figure 17, rather than the widely used monolithic architecture. These threads will run pre-emptively based on their priorities. This will allow critical tasks such as data acquisition and communication to be handled with top priority. It will also allow for asynchronous processing which enables low priority and time-consuming applications such as SD card writing to work with high priority tasks such as data acquisition from sensors, and communication with the host device.

DOI: 10.13009/EUCASS2019-504

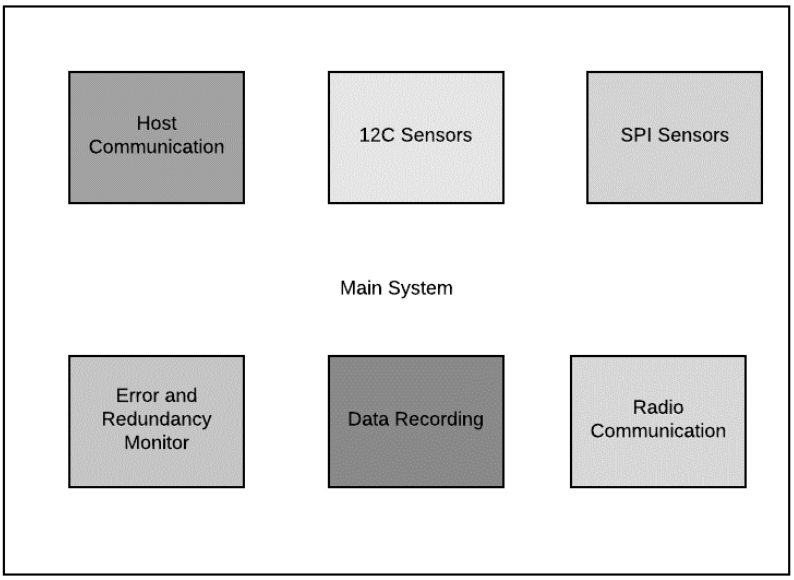

Figure 17 - Multi Threaded Embedded Architecture

6.Conclusion

The main propose of this paper was to provide a full design for a CubeSat Compatible Re-entry Capsule. Various methods such as engineering models, CFD analysis and structural analysis were performed to design the shape and structure of the craft in such way that the on-board equipment and experiments will be safe during the re-entry phase of the flight. Furthermore an on-board electronics suite was designed allowing for data collection, connection with the host cube sat, data retrieval and location beacon function to allow for the capsule to be recovered after re-entry.

References

[1] NASA, "Introduction," in *CubeSat101 - Basic Concepts and Processes for First-Time CubeSat Developers*, NASA, 2017, pp. 1-8.

[2] NASA, CubeSat101 - Basic Concepts and Processes for First-Time CubeSat Developers, NASA, 2017.

[3] J. D. Anderson and E. , Introduction to Flight, 7th ed., New York: McGraw Hill, 2012.

[4] R. D. Launius and D. R. Jenkins, Coming Home - Reentry and Recovery from Space, Washington DC: U.S. Government Printing Office, 2011.

[5] V. Carandente, R. Savino, M. Iacovazzo and C. Boffa, "Aerothermal Analysis of a Sample-Return Reentry Capsule," *FDMP*, vol. 9, no. 4, pp. 461-484, 2013.

[6] I. P. J. M. K. L. T. M. R. Maurizio Natali, "Microstructure and ablation behavior of an affordable and reliable nanostructured Phenolic Impregnated Carbon Ablator (PICA)," 2017.

[7] A. B. J.-P. B. R. T. J. F. D. G. B. G. F. G. F. H. R. H. M. K. G. K. N. M. R. M. A. J. R. V. S. H. S. M. S. V. S. M. Ehresmann, "CubeSat-sized Re-entry Capsule MIRKA2," in *10th IAA Symposium on Small Satellites for Earth Observation,*, Berlin, 2015.

DOI: 10.13009/EUCASS2019-504

[8] A. S. P. G. H. Jean-Pierre Baumann, "AerothermodynamicRe-entry Analysis of the CubeSat-sized Entry Vehicle MIRKA2Jean-Pierre Baumann (1), Adam S. Pagan (1) and Georg Herdrich (1)," in *8thEuropean Symposium on Aerothermodynamics for Space Vehicles*, Berlin, 2015.

[9] J.-P. B. G. H. Jaime Esper, "Cubesat Application for Planetary Entry (CAPE) Missions: Micro-Return Capsule (MIRCA)," in *30th Annual AIAA/USU Conference on Small Satellites*, Logan, 2016.

[10] Y. Takahashi and K. Yamada, "Aerodynamic heating of inflatable aeroshell in orbital reentry," *Acta Astronautica*, 2018.

[11] National Oceanic and Atmospheric Administration, "U.S. Standard Atmosphere, 1976," 01 October 1976. [Online]. Available: https://ntrs.nasa.gov/search.jsp?R=19770009539. [Accessed 11 November 2018].

[12] M. E. Tauber and K. Sutton, "Stagnation-Point Radiative Heating Relations for Earth and Mars Entries," *Journal of Spacecraft and Rockets*, vol. 28, no. 1, pp. 40-42, 1991.

[13] National Aeronautics and Space Administration, "Thermal and fluids analysis workshop (TFAWS)," 17 August 2012. [Online]. Available: https://tfaws.nasa.gov/TFAWS12/Proceedings/Aerothermodynamics%20Course.pdf. [Accessed 20 November 2018].

[14] R. W. Detra and H. Hidalgo, "Generalized Heat transfer formulas and graphs for nose cone re-entry into the atmosphere," *ARS Journal*, vol. 31, no. 3, pp. 318-321, 1961.

[15] A. P. Shafeeque, "CFD ANALYSIS ON AN ATMOSPHERIC RE-ENTRY MODULE," *International Research Journal of Engineering and Technology (IRJET)*, vol. 04, no. 1, pp. 587-594, 2017.

[16] ASM Aerospace Specification Metals Inc., "ASM Material Data Sheet," ASM Aerospace Specification Metals Inc. & Matweb, [Online]. Available: http://asm.matweb.com/search/SpecificMaterial.asp?bassnum=NTIME1023. [Accessed 10 February 2019].

[17] Morgan Advanced Materials, "Data Sheet - WDS Ultra," August 2016. [Online]. Available: http://www.morganthermalceramics.com/media/2631/wds-ultra-data-sheet-english-mi.pdf. [Accessed 10 April 2019].

[18] Active Space Technologies, "Aerogels - The future of thermal insulation for space applications," 2011. [Online]. [Accessed 2019 April 10].

[19] H. K. Tran, C. E. Johnson, D. J. Rasky, F. C. Hui, M.-T. Hsu, T. Chen, Y. K. Chen, D. Paragas and L. Kobayashi, "Phenolic Impregnated Carbon Ablators (PICA) as Thermal Protection Systems for Discovery Missions," National Aeronautics and Space Administration, 1997.

[20] RFSolutions-TF, "RF-LORA: The 50km Radio Module," DesignSpark, 25 April 2017. [Online]. Available: https://www.rs-online.com/designspark/rf-lora-the-50km-radio-module. [Accessed 11 November 2018].